https://doi.org/10.1016/j.jcsr.2023.107913

Classification system for inter- and intra-module joints in non-sway steel MiC structures

Xiao-Huang-Can He[a*], Tak-Ming Chan[b,c]

[a] School of Civil Engineering and Architecture, Guangxi University, Nanning, China

[b] Department of Civil and Environmental Engineering, The Hong Kong Polytechnic University, Hung Hom, Hong Kong, China

[c] Chinese National Engineering Research Centre for Steel Construction (Hong Kong Branch), The Hong Kong Polytechnic University, Hung Hom, Hong Kong, China

*Corresponding author: hxhc@gxu.edu.cn

Abstract

The lack of guidelines for determining the rigidity of inter- and intra-module joints in corner-supported steel modular integrated construction (MiC) buildings can lead to unsafe or over-conservative designs. To address this issue, this study proposes a classification system for non-sway steel MiC buildings that covers both inter- and intra-module joints. First, the semi-rigidity of the joint regions in steel MiC buildings was clarified and the necessary degrees of freedom for joint classification were determined. Then a minimum substructure including one joint region was extracted from a steel MiC building, and its carrying capacity was determined as a simplified analytical model that considering the stiffnesses of both the inter- and intra-module joints. The simplified model was adopted to derive explicit formulas for the boundary limits of rigid/non-rigid inter- and intra-module joints, based on the criterion that the carrying capacity of the substructure with finite joint stiffnesses is 95 percent of that with rigid properties. Finally, the feasibility of the proposed classification system was verified by applying it to prototype MiC structures.

Keywords: MiC structures; inter-module joints; intra-module beam-column joints; joint classification; boundary limits

1 Introduction

The modular integrated construction (MiC) method is an innovative, clean, and sustainable construction approach that can change the construction industry. Modules are manufactured in factories, transported to construction sites, and assembled individually by cranes. Thus, construction quality can be ensured, noise can be reduced, and construction waste can be minimized. This approach has been applied to temporary housing facilities, low-rise apartments [1], and high-rise buildings [2, 3].

There are generally two types of joints inside steel MiC structures: inter-module and intra-module joints. Inter-module joints combine different modules to form an entire building, whereas intra-module joints connect beams and columns inside each module [4]. Many researchers have studied the effect of inter-module joints on the structural behavior of steel MiC structures [4, 5]. For example, Farajian et al. [6] studied the effect of inter-module joints on the effective length of columns in steel MiC frames and found that the K-factor varies from 0.68 to 0.96 for non-sway modular structures. Zhai et al. [7] proposed a simplified equation for the K-factor of unbraced plate-type modular steel frames. Li et al. [8, 9] also discussed the effective length factor of braced and unbraced structures with different inter-modular joint stiffness values. Lacey et al. [10] studied the effect of inter-module joint stiffness on a modular building under wind and earthquake loadings and found that the shear stiffness of vertical inter-module joints has a greater effect on the inter-story drift ratio than the rotational stiffness does. Chua et al. [11] found that the lateral resistance of MiC buildings could be reduced owing to the relatively low tensile capacity and stiffness of vertical inter-module joints. Alembagheri et al. [12] investigated the

effect of inter-module joints on the progressive collapsing behavior of steel MiC structures. Srisangeerthanan et al. [13] inspected existing inter-module joints considering structural, manufacturing, and construction requirements.

Studies on the effects of intra-module joints are relatively limited. Styles et al. [14] investigated the effect of joint rotational stiffness on the response to wind loading of an 11-storey modular building. Accordingly, they found that increasing intra-module joint stiffness effectively reduced inter-story drift under wind load. He et al. [15] found that the configuration of inter-module joints could affect intra-module joints, which mainly affect the robustness of steel MiC structures.

During the design phase of steel MiC structures, it is important to determine the rigidity of both inter- and intra-module joints, which can be pinned, rigid, or semi-rigid[16]. Currently, in the UK, most MiC projects have adopted simple joints, such as fin plate and end-plate joints in the beam-column joints [4], and pinned assumption can be adopted for intra-module joints. In contrast, in most studies, it was assumed that the intra-module joints were fully rigid with adequate resistance [11, 17], as beams and columns are fully welded to each other. Although the current codes or guidelines [18, 19] for structural steel design have specified the boundaries for joint classification in beam-column joints, whether the joint classification limit for ordinary steel structures is suitable for steel MiC structures remains ambiguous, as they are derived based on the former type of structures. It is possible that existing approaches may yield a very conservative or uneconomical solution, and engineers must take significant risks to address the uncertainty and difference in the behavior compared to ordinary steel structures. Accordingly, Farajian et al. [20] proposed boundary limits for inter-modular connections in sway-corner-supported steel modular frames. They found that the boundary limits depended on the stiffness of the column

and beams, as well as the stiffness of the intra-module joints. However, they did not provide classification approaches for the shear behavior of the inter-module joints and the rotational behavior of the intra-module joints. Owing to the possible combined effect of inter- and intra-module joints, it is important to propose a joint classification approach that considers both inter- and intra-module joints to facilitate the design process.

Therefore, this study aims to investigate the effect of both inter- and intra-module joints on the carrying capacity of steel MiC structures subjected primarily to gravitational load and propose a boundary classification system for joint classification.

2 Methodology on joint classification

The structural performance of steel frame structures generally depends on the behavior of the beam-column joints. In reality, all joints possess neither an infinite stiffness value nor a zero one. To simplify the design and analysis processes, it is convenient to assume that a joint is either pinned or rigid, given that the properties of the joint satisfy the boundary criteria proposed in the design guidelines or other technical references. In this section, the joint classification methodology used in the literature for ordinary steel frame structures is demonstrated, and then that for steel MiC frame structures is introduced in a similar manner.

2.1 Joint classification for ordinary steel framed structures

It is well recognized that many beam-column joints possess semi-rigid properties that affect the structural behavior under load. Data on the joint properties were collected [21] and classification systems were proposed during the 1980s and 1990s [19, 22-24]. An ordinary steel-framed structure consists of numerous beam-column joints, as shown in Figure 1(a). The performance of the structure, denoted as F, such as the strength, displacement, and internal force, under different joint properties can be evaluated using the following equation

$$F = f(S, J_1, \ldots, J_N) \tag{1}$$

where "S" represents the structural configuration, including the span length, story height, member section sizes, etc., J_i represents the property of the i-th joint, and N is the total number of joints. Typically, only the rotational properties of these beam-column joints are considered in the design process.

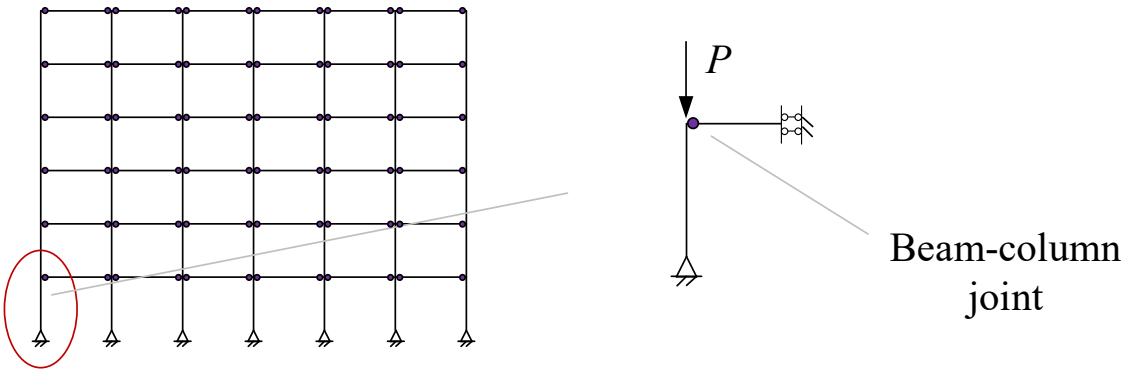

(a) (b)

Figure 1. Beam-column joint classification for traditional steel framed structures: (a) A steel frame; (b) the reference substructure adopted in EN 1993-1-8 (2005) for joint classification.

Using the relative parameters for the beam-column joints, Eq.(1) can be re-written as

$$F = f(S, \bar{S}_1, \ldots, \bar{S}_N) \tag{2}$$

where $\bar{S}_i$ is a non-dimensional scaling value and represents the stiffness of the i-th joint. $\bar{S}_i = 0$ denotes "pinned" and $\bar{S}_i = \infty$ denotes "rigid" joints. A joint i can be considered as "rigid" [25, 26] when

$$\left| \frac{f(S, \bar{S}_1, \ldots, \bar{S}_i, \ldots, \bar{S}_N) - f(S, \bar{S}_1, \ldots, \bar{S}_i = \infty, \ldots, \bar{S}_N)}{f(S, \bar{S}_1, \ldots, \bar{S}_i = \infty, \ldots, \bar{S}_N)} \right| \leq 0.05 \tag{3}$$

Denoting the boundary limit for joint i as B_i, it can be obtained by setting the left-hand side of Eq. (3) equal to the right-hand side:

$$B_i = b_i(S, \bar{S}_1, \dots, \bar{S}_{i-1}, \bar{S}_{i+1}, \dots, \bar{S}_{\mathrm{N}}) \tag{4}$$

where b_{i} is a function used to obtain the boundary limit. Note that the boundary limit B_{i} is not only determined by the structural system, S, but also by the properties of other joints. For all N joints, it is not practically possible to propose their boundary limits as they are intertwined. Therefore, it is usually assumed that all joints are simultaneously pinned or rigid. For example, if a rigid joint is assumed, its boundary limit can be obtained using the following equation

$$\left| \frac{f(S, \bar{S}_1, \dots, \bar{S}_{\mathrm{i}}, \dots, \bar{S}_{\mathrm{N}}) - f(S, \bar{S}_1 = \infty, \dots, \bar{S}_i = \infty, \dots, \bar{S}_{\mathrm{N}} = \infty)}{f(S, \bar{S}_1 = \infty, \dots, \bar{S}_i = \infty, \dots, \bar{S}_{\mathrm{N}} = \infty)} \right| = 0.05 \tag{5}$$

The boundary is a N-dimensional hyper-surface such that

$$B(\bar{S}_1, \dots, \bar{S}_{\mathrm{i}}, \dots, \bar{S}_{\mathrm{N}}) = b(S) \tag{6}$$

An N-dimensional hypersurface is inconvenient for engineering design. To simplify the procedure, the structural system is typically simplified such that only one joint is included. Figure 1(b) shows the simplified reference substructure adopted to derive the beam-column joint classification boundary limit in the EN 1993-1-8 (2005) standard [25, 27], in which only one beam-column joint is included. Similar approaches were adopted by Bjorhovde et al. [19] and Goto et al. [22]. Subsequently, the boundary surface is simplified to a scalar value

$$B = b(S_{\mathrm{sub}}, \bar{S}_1) \tag{7}$$

where S_{sub} represents the simplified substructure for joint classification. Then, the obtained boundary limit value was applied to the design and analysis of all joints.

Alternatively, the parameters of all the joints are assumed to be the same [26] as follows

$$\bar{S}_1 = \cdots = \bar{S}_i = \cdots = \bar{S}_{\mathrm{N}} = \bar{S} \tag{8}$$

Then, Eq.(2) becomes

$$F = f(S, \bar{S}_1, \dots, \bar{S}_{\mathrm{N}}) = f(S, \bar{S}) \tag{9}$$

123 The boundary can also be obtained as a scalar value, similar to Eq.(7). For braced steel structures,
124 the boundary limit between rigid and semi-rigid of beam-column joints is $8EI/L$, as specified in
125 EN 1993-1-8 (2005) standard [25].

126 ## 2.2 Semi-rigidity of joint region in steel MiC structures

127 Numerous inter-module joint types have been proposed in the literature [5, 28] for
128 assembling modules by using locking devices [29, 30], post-tensioned rods [11, 31, 32] or bolts
129 with different typologies [30, 33-39]; among them, single bolt or rod joints have been proposed
130 and studied experimentally and numerically by several researchers [11, 16, 29-32, 35], as shown
131 in Figure 2. The axial compressive force is transferred from the upper module to the lower
132 module by the hollow steel section, whereas the possible axial tensile force is transferred solely
133 by the single rod or bolt. The shear force between the modules can be resisted by an added shear
134 key, as shown in Figure 2(a), 2(b), and 2(c), or by the bolt itself, as shown in Figure 2(d), 2(e),
135 and 2(f). The moment resistance is provided by the coupling effect between the tensile rod or
136 bolt and one side wall of the compressed columns owing to the contact effect. The horizontal
137 joint between the modules can be realized using an added intermediate plate, as shown in Figure
138 2(c).

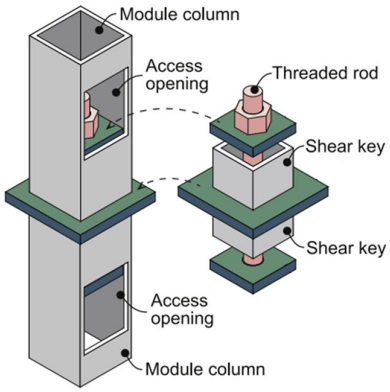

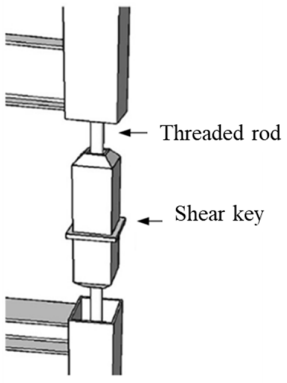

(a) Rod joint with shear key [31]

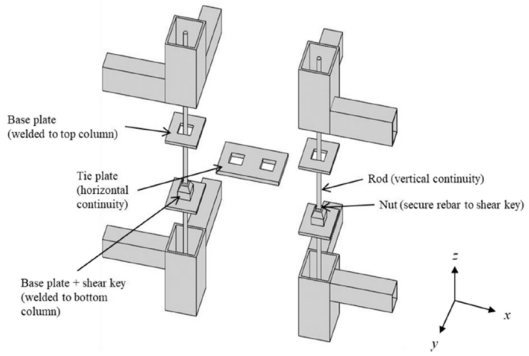

(b) Rod joint with shear key [32]

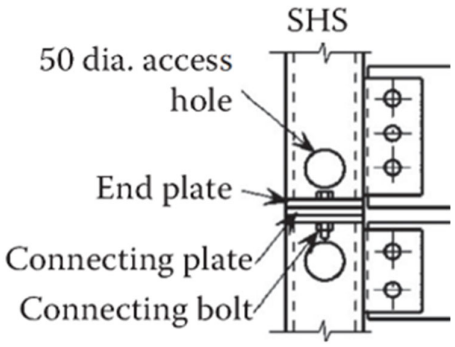

(c) Rod joint with shear key [11]

(d) Bolt joint [35]

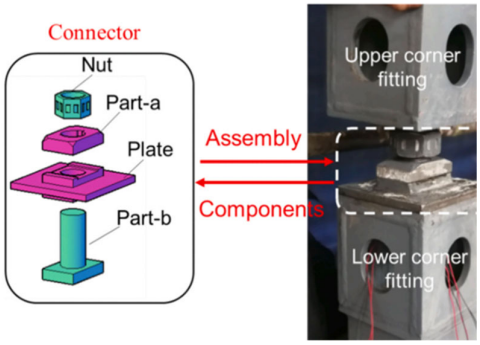

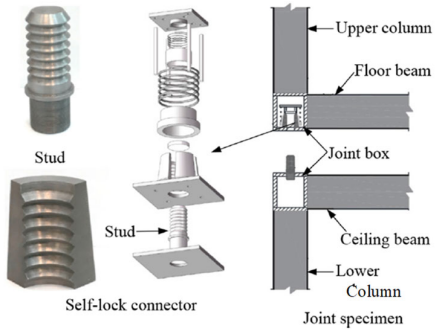

(e) Bolt joint [30]

(f) Bolt joint[29]

Figure 2. Inter-module joints consisting of a single rod or bolt

For intra-module joints, modular beams can be fully welded to modular columns, as shown in parts (b), (c), and (f) of Figure 2. In addition, a corner fitting [30] or a strong corner bloc [40] may be used near rigid joints. Alternatively, the simple shear connection shown in Figure 2(d) can be applied.

Figure 3 shows a typical joint region in steel MiC structures using a single bolt connection that can be modelled using intra- and inter-model joints [41]. The intra-module joints include beam-column joints for the floor and ceiling beams; the respective rotational stiffness values are denoted as S_{FR} and S_{CR}. It should be noted even when modular beams are fully welded to the

columns in the factory, the intra-module joints can behave in a non-rigid manner due to a lack of endplates or stiffeners inside the columns [15, 39].Therefore, it is necessary to classify the intra-module joints.

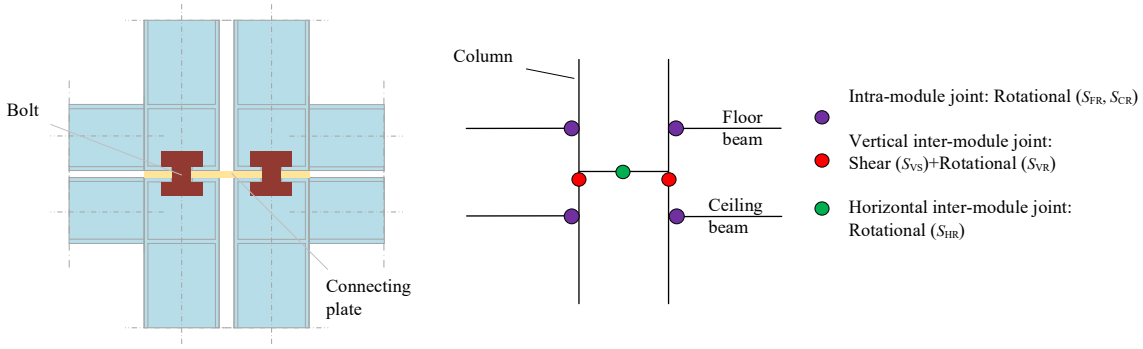

Figure 3. Typical joint region in the steel MiC structure and its simplified model.

Each vertical inter-module joint consists of axial, shear, and rotational behaviors, which can be denoted as S_{VA}, S_{VS}, S_{VR}, respectively. The axial behavior is determined by the mechanical behavior of the bolt in tension and compressive contact of the upper and lower columns. Under gravity loading conditions, the compressive stiffness is comparable to the area of the column section; therefore, a rigid assumption can be used. The shear behavior is affected by the slip-contact behavior between the bolts and columns; therefore, a shear spring should be incorporated in the joint region. The rotational behavior is determined by the coupling effect between the bolt and one side of the end surface of the column, which is denoted as S_{VR} in Figure 3. Therefore, only S_{VS} and S_{VR} will be considered in the model.

Each horizontal inter-module joint consists of axial, shear, and rotational behaviors, which can be denoted as S_{HA}, S_{HS}, S_{HR}, respectively. The axial behavior is determined by the axial strength of the connecting plate, which is usually assumed to be rigid. Because of symmetry, the shear behavior can be omitted, thus, only the rotational stiffness S_{HR} is included in the joint region, as shown in Figure 3. The simplified joint model is also applicable for inter-module

connections[33, 34, 36, 37] using bolts to connect the lower and upper columns and one intermediate plate to connect the left and right modules.

2.3 Joint classification for steel MiC structures

As discussed in section 2.2, a typical joint region of steel MiC structures comprises inter- and intra-module joints, and the inter-module joints can be further classified as vertical and horizontal inter-module joints, whereas the intra-module joints can be further classified as floor beam-column joints and ceiling beam-column joints. Under gravity loading conditions, the stiffness values S_{FR}, S_{CR}, S_{VA}, S_{VS}, and S_{VR} are identified as the most critical joint parameters in steel MiC structures. And a classification system for these five joint parameters should be proposed.

To propose the classification system, a reference substructure of typical steel MiC structures with only one joint region including the five joint parameters is used for performance evaluation. When determining the boundary limit for each joint behavior parameter, the reference substructure is further simplified such that all other joint behavior parameters are either pinned or rigid. Then the boundary limit can be obtained as a scalar value, similar to Eq.(7). The methodology for both inter- and intra-module joint classification for steel MiC structures is as follows:

1. Select a simplified reference substructure where both inter- and intra-module joints are included and identify the joint modelling parameters.

2. Derive the structural performance evaluation approach of the substructure with different joint parameter values.

3. Carry out sensitivity analysis on these joint parameters. For each joint parameter, determine the critical joint configurations for the other joint parameters (pinned or rigid) such

that only this joint parameter is incorporated when evaluating the structural performance. In the critical joint configuration, varying the value of this joint parameter underlines the greatest difference in structural performance. Therefore, all joint parameters are decoupled in this manner.

4. Derive the boundary limit for each joint parameter. The boundary limit value is determined when the structural performance of the substructure is 95% of that when the joint parameter value is very large (10000).

In the following, a reference substructure and carrying capacity evaluation approach to assess structural performance are demonstrated in Section 3. Subsequently, the effect of joint behavior on the structural performance is investigated, and the critical joint configuration for each joint parameter is determined. Then, the boundary limits for all five joint parameters are proposed, followed by two examples to verify their effectiveness.

3 Reference structure and evaluation of carrying capacity

3.1 Reference substructure

In multi-story or high-rise steel MiC structures, the pure module part can be designed to resist gravity loading only, while the lateral resistance is provided by the concrete core or steel bracing system by approximately 95% [11], as shown in Figure 4(a). Therefore, we assumed that the critical failure mode is column buckling at the bottom story because the column size is similar for consecutive stories. Moreover, the column of the bottom story carries the largest loading, and the consequence of column buckling is more serious than that of beam failure. Therefore, the module at the bottom story with a half module from the second story was used as the reference substructure to consider the effect of the inter- and intra-module joints, as shown in Figure 4(b). The height and length of a module is denoted as H and L, respectively. The joints in the base module were assumed to be pinned. By utilizing symmetry, half of the

substructure was built, consisting of two floor beams, one ceiling beam, and two columns. The right ends of the floor beams and ceiling were restrained horizontally and rotationally, respectively. The left end of the horizontal inter-module joint was also restrained horizontally and rotationally. The top end of the column in the second story was horizontally restrained assuming that it was the point of contra-flexure.

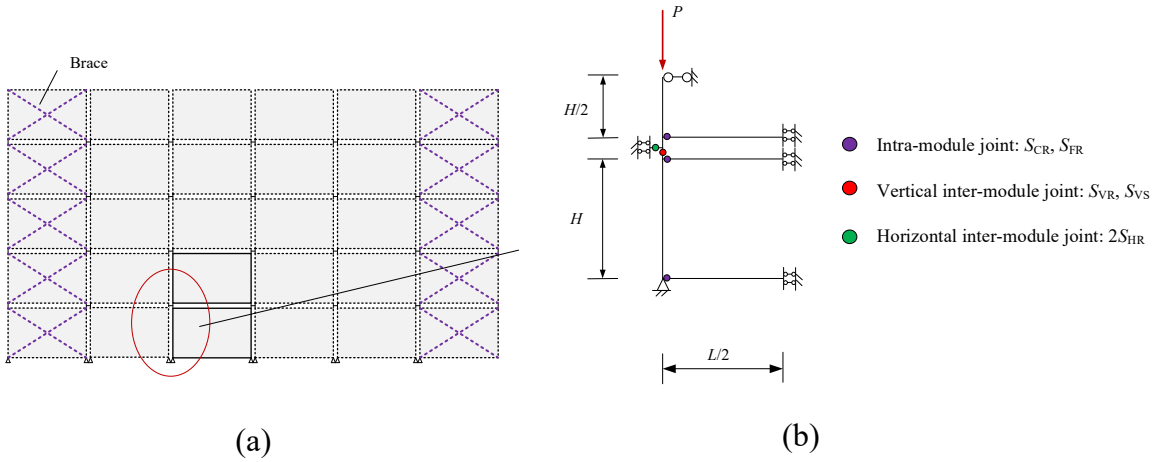

Figure 4. (a) Reference substructure in a braced steel MiC frame; (b) details of the substructure and joint modelling.

The carrying capacity of the reference substructure is evaluated by varying the different properties of intra- and inter-module joint stiffness. The carrying capacity is defined as the maximum axial force (N_u) in the modular column during loading.

3.2 Evaluation of carrying capacity

The capacity of the reference structure can be evaluated through the carrying capacity of the bottom modular column, as shown in Figure 5, restrained by a rotational spring with stiffness R_A at the bottom and another at the top with stiffness R_B. The carrying capacity of the substructure N_u is approximated using the Merchant-Rankine formula [42]

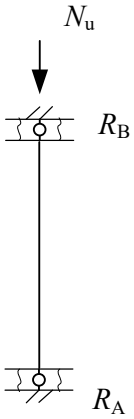

229

230 Figure 5. Sketch used to determine the carrying capacity of a column.

$$N_u = \left(\frac{1}{N_p} + \frac{1}{N_{cr}}\right)^{-1} \tag{10}$$

231 where N_p is the axial compressive capacity of the column, which can be calculated as

$$N_p = A_c f_y \tag{11}$$

232 where A_c is the sectional area of the column and f_y is the yield strength of the column material.

233 N_{cr} is the Euler critical load, which can be calculated as

$$N_{cr} = \frac{\pi^2 E I_c}{(KH)^2} \tag{12}$$

234 where K is the effective length ratio, E is the elastic modulus, and I_c is the second moment of

235 area of the column. The slenderness of the column is denoted as

$$\bar{\lambda} = N_p / N_{cr} \tag{13}$$

236 Furthermore, denote $\bar{\lambda}_0$ as the slenderness of the column when the two ends are pinned

237 connected. Then it is easy to obtain

$$\bar{\lambda} = K\bar{\lambda}_0 \tag{14}$$

238 Substitute Eqs.(13) and (14) into Eq.(10), the carrying capacity N_u can be re-written as [43]

$$N_{\mathrm{u}} = N_{\mathrm{p}} \frac{1}{1 + K^2 \bar{\lambda}_0^2} \tag{15}$$

According to Jaspart et al. [43], K can be calculated as

$$K = \frac{1 + 0.145(k_{\mathrm{l}} + k_{\mathrm{u}}) - 0.265 k_{\mathrm{l}} k_{\mathrm{u}}}{2 - 0.364(k_{\mathrm{l}} + k_{\mathrm{u}}) - 0.247 k_{\mathrm{l}} k_{\mathrm{u}}} \tag{16}$$

where

$$k_{\mathrm{l}} = \frac{4}{4 + \bar{R}_{\mathrm{A}}}, k_{\mathrm{u}} = \frac{4}{4 + \bar{R}_{\mathrm{B}}} \tag{17}$$

where $\bar{R}_{\mathrm{A}}$ and $\bar{R}_{\mathrm{B}}$ are

$$\bar{R}_{\mathrm{A}} = R_{\mathrm{A}}/i_{\mathrm{c}}, \bar{R}_{\mathrm{B}} = R_{\mathrm{B}}/i_{\mathrm{c}} \tag{18}$$

In Eq. (18), $i_{\mathrm{c}} = EI_{\mathrm{c}}/H$ is the bending stiffness of the column element. The values of R_{A} and R_{B} are described in Section 3.3.

3.3 Rotational restraints of the bottom modular column ends

The relative stiffness values of the intra-module floor beam-column joint and intra-module ceiling beam-column joint are denoted as

$$\bar{S}_{\mathrm{FR}} = S_{\mathrm{FR}}/i_{\mathrm{fb}}, \bar{S}_{\mathrm{CJ}} = S_{\mathrm{CJ}}/i_{\mathrm{cb}} \tag{19}$$

where $i_{\mathrm{fb}} = EI_{\mathrm{fb}}/L$ and $i_{\mathrm{cb}} = EI_{\mathrm{cb}}/L$ are the element bending stiffnesses of the column, floor beam, and ceiling beam, respectively, and I_{fb}, and I_{cb} are the second moments of area for the sections of the floor beam and the ceiling beam, respectively.

The relative stiffnesses values of horizontal and vertical inter-module joint are denoted as

$$\bar{S}_{\mathrm{HR}} = S_{\mathrm{HR}}/i_{\mathrm{c}}, \bar{S}_{\mathrm{VR}} = S_{\mathrm{VR}}/i_{\mathrm{c}}, \bar{S}_{\mathrm{VS}} = S_{\mathrm{VS}}/k_{\mathrm{cb}} \tag{20}$$

where S_{HR} and S_{VR} are the stiffnesses of the horizontal and vertical rotational joints, respectively, and S_{VS} is the shear stiffness of the vertical inter-module joint. k_{cb} is the axial stiffness of the ceiling beam, which can be calculated as

$$k_{\mathrm{cb}} = EA_{\mathrm{cb}}/L \tag{21}$$

where A_{cb} is the cross-section area of the ceiling beam.

For the column bottom end, as shown in Figure 5, the rotational restraint stiffness originates from the floor beam and intra-module floor beam-column joint; therefore, it can be calculated as

$$R_{\mathrm{A}} = \frac{S_{\mathrm{FR}} \cdot 2i_{\mathrm{fb}}}{S_{\mathrm{FR}} + 2i_{\mathrm{fb}}} = \frac{2\bar{S}_{\mathrm{FR}} i_{\mathrm{c}} i_{\mathrm{fb}}}{\bar{S}_{\mathrm{FR}} i_{\mathrm{c}} + 2i_{\mathrm{fb}}} \tag{22}$$

Divided by i_{c}, the above equation becomes

$$\bar{R}_{\mathrm{A}} = \frac{2\bar{S}_{\mathrm{FR}} i_{\mathrm{fb}}/i_{\mathrm{c}}}{\bar{S}_{\mathrm{FR}} + 2i_{\mathrm{fb}}/i_{\mathrm{c}}} \tag{23}$$

For the column top end, as shown in Figure 5, the rotational restraint stiffness originates from the inter- and intra-module joint region at the top and the module at the second story. To determine the rotational stiffness, the joint region was extracted from Figure 5 in detail, as shown in Figure 6(a) and (b). The two short column stubs between the floor beam and ceiling beam were modelled as rigid beams, that is, with infinite axial and bending stiffness. The bottom end (node 1) of the lower short column stub was restrained by a translational spring and rotational spring with stiffnesses equal to k_1 and r_1, respectively. The top end (node 2) of the upper short column stub was restrained by a translational spring and rotational spring with stiffnesses equal to k_2 and r_2, respectively. The two short column stubs are connected at nodes 3 and 4 by a translational spring and a rotational spring with stiffnesses equal to k_3 and r_3, respectively. In addition, the lower end of the upper short column (node 4) was restrained by a rotational spring with a stiffness equal to r_4 and translational movement was prevented.

The value of k_1 originates from the axial stiffness of the ceiling beam, which can be calculated as

$$k_1 = 2k_{\mathrm{cb}} \tag{24}$$

The value of r_1 originates from the combined rotational effect of the intra-module ceiling beam-column joint and the bending stiffness of the ceiling beam, which can be calculated as

$$r_1 = \frac{S_{\mathrm{CR}} \cdot 2i_{\mathrm{cb}}}{S_{\mathrm{CR}} + 2i_{\mathrm{cb}}} = \frac{2\bar{S}_{\mathrm{CR}} i_{\mathrm{c}} i_{\mathrm{cb}}}{\bar{S}_{\mathrm{CR}} i_{\mathrm{c}} + 2i_{\mathrm{cb}}} \tag{25}$$

n

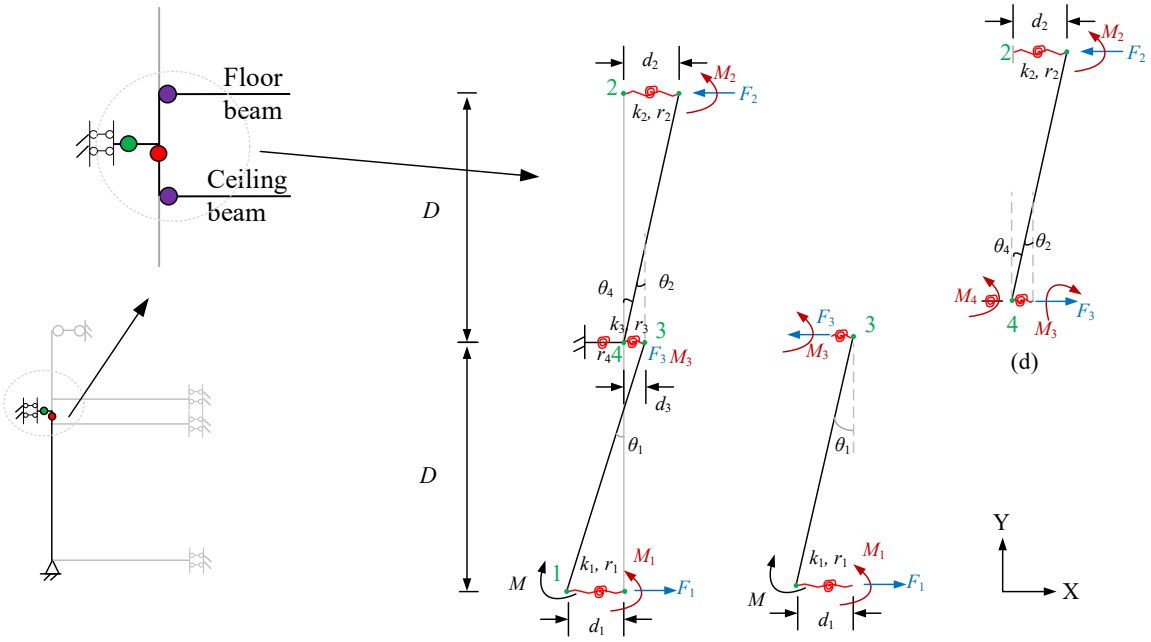

Figure 6. Sketch used to determine the rotational stiffness at the top end of the bottom column.

The value of k_2 originates from the axial stiffness of the floor beam, which can be calculated as

$$k_2 = 2k_{\mathrm{fb}} \tag{26}$$

where k_{fb} is the axial stiffness of the ceiling beam and can be calculated as

$$k_{\mathrm{fb}} = EA_{\mathrm{fb}}/L \tag{27}$$

where A_{fb} is the section area of the floor beam.

The value of r_2 originates from the combined rotational effect of the intra-module floor beam-column joint and the bending stiffness of the floor beam, as well as the column on the second floor, which can be calculated as

$$r_2 = \frac{2\bar{S}_{\mathrm{FR}} i_{\mathrm{c}} i_{\mathrm{fb}}}{\bar{S}_{\mathrm{FR}} i_{\mathrm{c}} + 2i_{\mathrm{fb}}} + 6i_{\mathrm{c}} \tag{28}$$

The value of k_3 represents the shear stiffness of the vertical inter-module joints, which can be calculated as

$$k_3 = S_{\mathrm{VS}} = \bar{S}_{\mathrm{VS}} k_{\mathrm{cb}} \tag{29}$$

The value of r_3 represents the rotational stiffness of the vertical inter-module joint, which can be calculated as:

$$r_3 = S_{\mathrm{VR}} = \bar{S}_{\mathrm{VR}} i_{\mathrm{c}} \tag{30}$$

The value of r_4 represents the rotational stiffness of the horizontal inter-module joint, which can be calculated as

$$r_4 = 2S_{\mathrm{HR}} = 2\bar{S}_{\mathrm{HR}} i_{\mathrm{c}} \tag{31}$$

Factor 2 considers that only half of the horizontal inter-modular joint is modelled in the substructure.

It is defined that d_{i} (i = 1, 2, 3) is the displacement corresponding to the translational spring with stiffness k_{i} and θ_{i} is the displacement corresponding to the rotational spring with stiffness r_{i} (i = 1, 2, 3, 4). Then, the forces and moments in the springs are

$$F_i = k_i d_i, i = 1, 2, 3 \tag{32}$$

and

$$M_i = r_i\theta_i, i = 1, 2, 3, 4 \tag{33}$$

298 Given a rotational angle $\theta_1 = \theta$ at the top of the bottom modular column (node 1), the
299 deformation shape and corresponding reaction forces are shown in Figure 6(c). According to
300 the geometrical compatibility, it is easy to determine that

$$\theta_3 = \theta_1 - \theta_2 \tag{34}$$

301

$$\theta_4 = \theta_2 \tag{35}$$

302

$$d_2 = \theta_2 D \tag{36}$$

303

$$d_3 = \theta_1 D - d_1 \tag{37}$$

304 According to the force equilibrium in the X-direction, as shown in Figure 6(c),

$$F_1 - F_3 = 0 \tag{38}$$

305 According to the moment equilibrium at node 1, as shown in Figure 6(c):

$$M - (M_1 + M_3 + F_3 D) = 0 \tag{39}$$

306 According to the moment equilibrium at node 4, as shown in Figure 6(d):

$$M_3 - (M_2 + F_2 D + M_4) = 0 \tag{40}$$

307 By substituting Eqs. (32)–(37) into Eqs.(38)–(40), it is obtained:

$$M = R_{\mathrm{B}}\theta_1 \tag{41}$$

308 where

$$R_{\mathrm{B}} = \frac{(r_1 r_2 + r_1 r_3 + r_1 r_4 + r_2 r_3 + r_3 r_4)}{(k_2 D^2 + r_2 + r_3 + r_4)} + \frac{D^2\begin{pmatrix} D^2 k_1 k_2 k_3 + k_1 k_2 (r_1 + r_3) + k_1 k_3 (r_2 + r_3) \\ + k_2 k_3 (r_1 + r_3) + k_1 k_3 r_4 \end{pmatrix}}{(k_1 + k_3)(k_2 D^2 + r_2 + r_3 + r_4)} \tag{42}$$

Subsequently, the rotational restraint factor $\bar{R}_B$ can be calculated. The effective length ratio of the bottom modular column can be obtained using Eqs. (16) and (17). Then the carrying capacity of the substructure was calculated using Eq. (10) or (15).

4 Effect of inter- and intra-module joints on the carrying capacity and proposal of boundary limits

4.1 Settings for the sensitivity analysis

Let the module length (L) be 5 m and the modular height (H) be 3 m. Five sections of the columns are considered, namely, SHS 90×5, SHS 100×6, SHS 120×6.3, SHS 160×8, and SHS 220×10. The corresponding values of $\overline{\lambda_0}$ are 1.15, 1.04, 0.86, 0.64, and 0.46, respectively. Two sections of the floor beam are considered, namely, RHS 140×80×8 and RHS 200×100×10. Two sections of the ceiling beam are SHS 80×80×5 and RHS 140×80×8. The properties of these members are listed in Table 1.

Table 1. Geometrical information and properties of the member

Member	Section type	Area (mm^2)	Second moment of area (10^6 mm^4)	Plastic compressive resistance (kN)	Bending resistance (kN-m)	Stiffness EI/L (EI/H) (kN-m)	Axial stiffness EA/L^* (kN/m)
Floor beam	RHS 140×80×8	3195	7.763	1134.34	50.04	320	131634
	RHS 200×100×10	5493	26.64	1949.91	144.92	1785	226311
Ceiling beam	SHS 80×80×5	1436	1.314	509.64	14.11	88	59163
	RHS 140×80×8	3195	7.763	1134.34	50.04	320	131634
Column	SHS 90×5	1673	1.996	593.98	18.81	137	/
	SHS 100×6.3	2319	3.356	823.12	28.71	230	/

	SHS 120×6.3	2823	6.029	1002.04	42.47	414	/
	SHS 160×8	4795	18.31	1702.34	96.49	1257	/
	SHS 220×10	8293	60.50	2943.91	230.68	4154	/

322

323 The effects of $\bar{S}_{\mathrm{HR}}$, $\bar{S}_{\mathrm{VS}}$, $\bar{S}_{\mathrm{VR}}$, $\bar{S}_{\mathrm{FR}}$, and $\bar{S}_{\mathrm{CR}}$ on carrying capacity were independently
324 investigated. Four values for the joint parameters were selected, namely, 0, 1, 10, and 10000,
325 where the pinned, semi-rigid, and rigid conditions were considered. The five column sections,
326 two floor beam sections, and two ceiling beam sections were adopted. When investigating the
327 effect of one joint parameter, for example, $\bar{S}_{\mathrm{HR}}$, 5120 ($4 \times 4 \times 4 \times 4 \times 5 \times 2 \times 2 = 5120$)
328 configurations of the structure were set. For each configuration, the value of $\bar{S}_{\mathrm{HR}}$ was varied
329 from 0, 0.1, 0.2, 0.3, 0.4, 0.5, 0.6, 0.7, 0.8, 0.9, 1, 1.2, 1.4, 1.6, 1.8, 2, 2.5, 3, 3.5, 4, 4.5, 5, 5.5,
330 6, 6.5, 7, 7.5, 8, 8.5, 9, 9.5, 10, 12, 14, 16, 18, 20, 50, 100, 1000, to 10000. Subsequently, the
331 corresponding carrying capacity N_{u} was obtained. The relative capacity is defined as

$$\frac{N_{\mathrm{u}}}{N_{\mathrm{u,rigid}}} = \frac{f(\overline{\lambda_0}, i_{\mathrm{fb}}, i_{\mathrm{cb}}, k_{\mathrm{fb}}, k_{\mathrm{cb}}, \bar{S}_{\mathrm{HR}}, \bar{S}_{\mathrm{VR}}, \bar{S}_{\mathrm{VS}}, \bar{S}_{\mathrm{FR}}, \bar{S}_{\mathrm{CR}})}{f(\overline{\lambda_0}, i_{\mathrm{fb}}, i_{\mathrm{cb}}, k_{\mathrm{fb}}, k_{\mathrm{cb}}, \bar{S}_{\mathrm{HR}} = 10000, \bar{S}_{\mathrm{VR}}, \bar{S}_{\mathrm{VS}}, \bar{S}_{\mathrm{FR}}, \bar{S}_{\mathrm{CR}})} \tag{43}$$

332 where $N_{\mathrm{u,rigid}}$ denotes the carrying capacity when $\bar{S}_{\mathrm{HR}}$ is 10000.

333 ## 4.2 Effect of inter- and intra-module joints on the carrying capacity

334 Figure 7 and Figure 8 show the effect of inter- and intra-module joints, respectively, on
335 the carrying capacity with different column sections. The main findings are the following:

336 1. For some joint configurations, the carrying capacity varied significantly as the stiffness
337 ratio, $\bar{S}_{\mathrm{HR}}$, $\bar{S}_{\mathrm{VR}}$, $\bar{S}_{\mathrm{VS}}$, $\bar{S}_{\mathrm{FR}}$, or $\bar{S}_{\mathrm{CR}}$ changed. The smallest relative capacity values were
338 approximately 0.93, 0.80, 0.71, 0.75, and 0.80 when individually varying $\bar{S}_{\mathrm{HR}}$, $\bar{S}_{\mathrm{VR}}$, $\bar{S}_{\mathrm{VS}}$, $\bar{S}_{\mathrm{FR}}$,
339 and $\bar{S}_{\mathrm{CR}}$, while the column section SHS 90×5 is adopted and the varied stiffness value is zero.

Therefore, assuming rigidity for all joint parameters will yield unsafe results, and assuming all joint parameters as pinned will yield over-conservative results.

2. There is a general trend that as the size of the column section or column slenderness $\overline{\lambda_0}$ increases, the effect of the joint parameter decreases. This could be anticipated because the carrying capacity of a modular column would increase if the effect of the boundary constraint increases. When the column section was relatively strong, such as in SHS 220×10, the carrying capacity did not vary significantly, because the strength reduction factor of the column with both ends pinned was already 0.95, which means that the column is a robust member and its carrying capacity could not be increased any further by increasing the restraint effect. If 0.95 is the boundary limit where the rigid assumption can be used, the boundary limit values for all the five joint parameters decrease. The effects of $\bar{S}_{\mathrm{HR}}$, $\bar{S}_{\mathrm{VR}}$ and $\bar{S}_{\mathrm{CR}}$ can be ignored when $\overline{\lambda_0}$ is smaller than or equal to 0.64, while the effect $\bar{S}_{\mathrm{FR}}$ can be ignored when $\overline{\lambda_0}$ is smaller than or equal to 0.46.

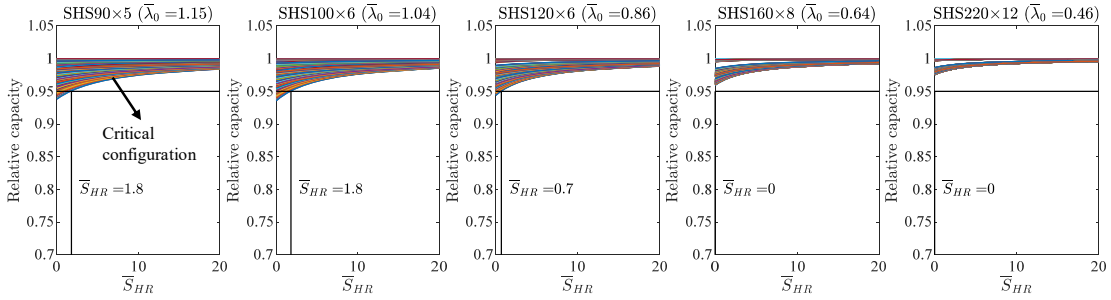

(a) Effect of $\bar{S}_{\mathrm{HR}}$

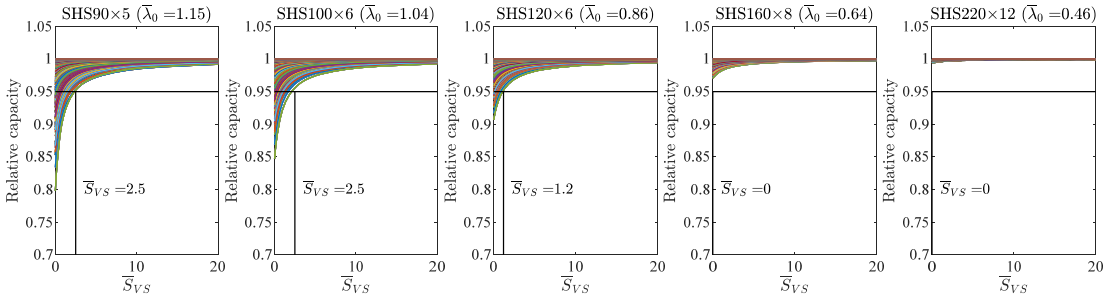

(b) Effect of $\bar{S}_{\mathrm{VS}}$

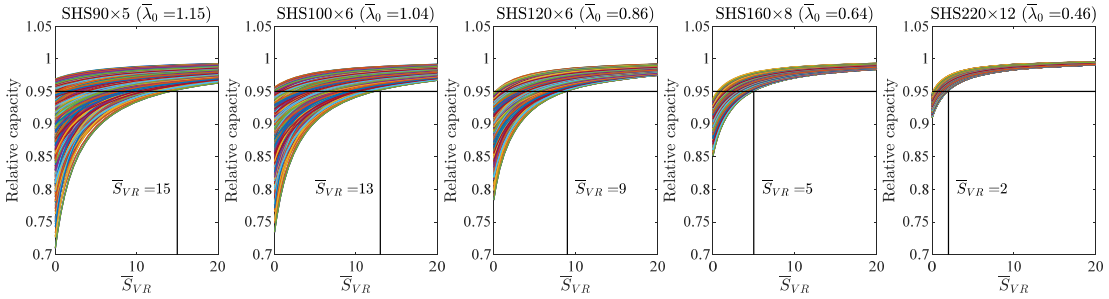

(c) Effect of $\bar{S}_{\mathrm{VR}}$

353 Figure 7. Effect of inter-module joints on the carrying capacity.

354

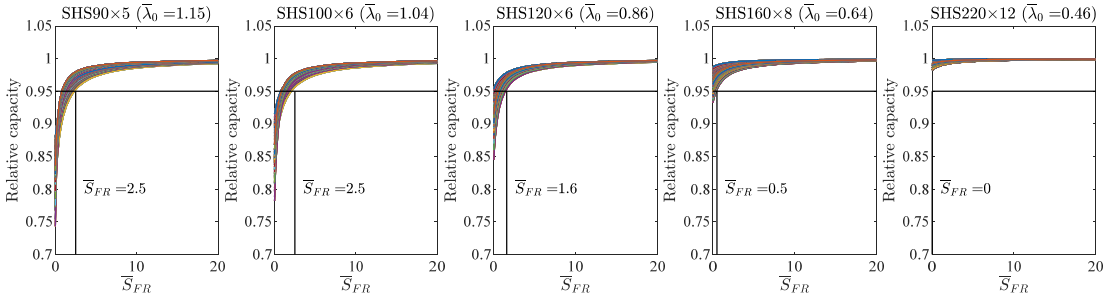

(a) Effect of $\bar{S}_{\mathrm{FR}}$

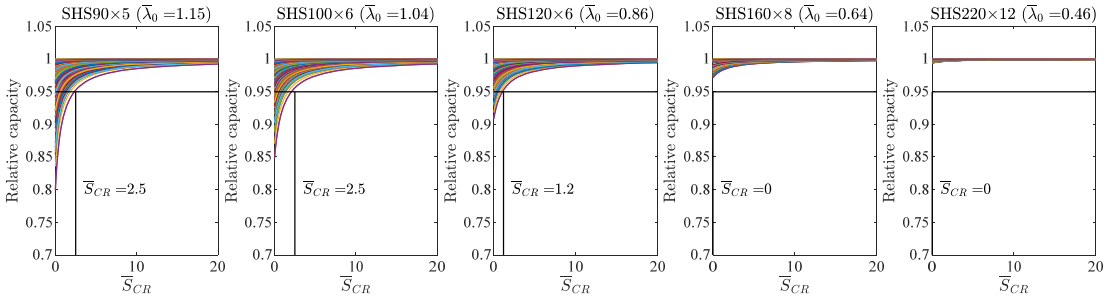

(b) Effect of $\bar{S}_{\mathrm{CR}}$

Figure 8. Effect of intra-module joints on the carrying capacity.

The boundary limit values between the rigid and non-rigid joints for all five joint parameters are listed in Table 2.

Table 2. Rigid and non-rigid boundary values for $\bar{S}_{\mathrm{HR}}$, $\bar{S}_{\mathrm{VR}}$, $\bar{S}_{\mathrm{VS}}$, $\bar{S}_{\mathrm{FR}}$, $\bar{S}_{\mathrm{CR}}$ by sensitivity analysis

	SHS 90×5 ($\bar{\lambda}_0 = 1.15$)	SHS 100×6.3 ($\bar{\lambda}_0 = 1.04$)	SHS 120×6.3 ($\bar{\lambda}_0 = 0.86$)	SHS 160×8 ($\bar{\lambda}_0 = 0.64$)	SHS 220×10 ($\bar{\lambda}_0 = 0.46$)
$\bar{S}_{\mathrm{HR}}$	1.8	1.8	0.7	0	0
$\bar{S}_{\mathrm{VS}}$	2.5	2.5	0.6	0	0
$\bar{S}_{\mathrm{VR}}$	15	13	9	5	2
$\bar{S}_{\mathrm{FR}}$	2.5	2.5	1.6	0.5	0
$\bar{S}_{\mathrm{CR}}$	2.5	2.5	1.2	0	0

4.3 Derivation of boundary limit curves

According to the sensitivity analysis, the critical joint configurations, that is, the curves that indicate the greatest effect for each joint parameter, are listed in Table 3. Using the critical values listed in the table, the column-end rotational restraint factors $\bar{R}_{\mathrm{A}}$ and $\bar{R}_{\mathrm{B}}$ can be calculated, as reported in the last two columns in Table 3.

Table 3. Critical configuration for different joint parameters and corresponding rotational

restraint factors for the column end

	$\bar{S}_{\mathrm{HR}}$	$\bar{S}_{\mathrm{VS}}$	$\bar{S}_{\mathrm{VR}}$	$\bar{S}_{\mathrm{FR}}$	$\bar{S}_{\mathrm{CR}}$	$\bar{R}_{\mathrm{A}}$	$\bar{R}_{\mathrm{B}}$
Effect of $\bar{S}_{\mathrm{HR}}$	\	10000	0	0	0	0	$6+2\bar{S}_{\mathrm{HR}}+2k_{\mathrm{fb}}D^2/i_{\mathrm{c}}$
Effect of $\bar{S}_{\mathrm{VS}}$	0	\	0	0	0	0	$2\bar{S}_{\mathrm{VS}}k_{\mathrm{cb}}D^2/i_{\mathrm{c}}(2+\bar{S}_{\mathrm{VS}})$
Effect of $\bar{S}_{\mathrm{VR}}$	10000	0	\	0	0	0	$\bar{S}_{\mathrm{VR}}$
Effect of $\bar{S}_{\mathrm{FR}}$	0	Any	0	\	0	$2\bar{S}_{\mathrm{FR}}i_{\mathrm{fb}}/i_{\mathrm{c}}(\bar{S}_{\mathrm{FR}}+2)$	0
Effect of $\bar{S}_{\mathrm{CR}}$	Any	0	0	0	\	0	$2\bar{S}_{\mathrm{CR}}i_{\mathrm{cb}}/i_{\mathrm{c}}(\bar{S}_{\mathrm{CR}}+2)$

It was found that one of the two factors, $\bar{R}_{\mathrm{A}}$ and $\bar{R}_{\mathrm{B}}$, was zero and the other was a function of the joint parameter. Denoting the non-zero factor as *u*, it is obtained

$$\begin{cases} u_{\mathrm{HR}}=6+2\bar{S}_{\mathrm{HR}}+2k_{\mathrm{fb}}D^2/i_{\mathrm{c}} \\ u_{\mathrm{VS}}=2\bar{S}_{\mathrm{VS}}k_{\mathrm{cb}}D^2/i_{\mathrm{c}}(2+\bar{S}_{\mathrm{VS}}) \\ u_{\mathrm{VR}}=\bar{S}_{\mathrm{VR}} \\ u_{\mathrm{FR}}=2\bar{S}_{\mathrm{FR}}i_{\mathrm{fb}}/i_{\mathrm{c}}(\bar{S}_{\mathrm{FR}}+2) \\ u_{\mathrm{CR}}=2\bar{S}_{\mathrm{CR}}i_{\mathrm{cb}}/i_{\mathrm{c}}(\bar{S}_{\mathrm{CR}}+2) \end{cases} \tag{44}$$

where the subscripts "HR," "VS," "VR," "FR," "CR" represent the five joint parameters. Therefore, the boundary limits for these joint parameters can be derived in a similar manner.

For the substructure shown in Figure 5, the criterion between the rigid and semi-rigid vertical inter-module joints is that the carrying load should be at least 95% of the loading capacity

$$\frac{N_{\mathrm{u}}}{N_{\mathrm{u,rigid}}}=\frac{1+K_{\mathrm{rigid}}^2\bar{\lambda}_0^2}{1+K^2\bar{\lambda}_0^2}\geq 0.95 \tag{45}$$

Or

$$K\leq\sqrt{\frac{0.05+K_{\mathrm{rigid}}^2\bar{\lambda}_0^2}{0.95\bar{\lambda}_0^2}} \tag{46}$$

In Eqs.(45) and (46), K_{rigid} is the effective length ratio of the column when the joint parameter is ∞ and K is the effective length ratio of the column when the joint parameter is finite. They can be obtained by

$$K = \frac{1 + 0.145\frac{8}{4+u} - 0.265\frac{4}{4+u}}{2 - 0.364\frac{8}{4+u} - 0.247\frac{4}{4+u}} \tag{47}$$

and

$$K_{\text{rigid}} = \frac{1 + 0.145\frac{8}{4+u_{\text{rigid}}} - 0.265\frac{4}{4+u_{\text{rigid}}}}{2 - 0.364\frac{8}{4+u_{\text{rigid}}} - 0.247\frac{4}{4+u_{\text{rigid}}}} \tag{48}$$

where u can be obtained using Eq.(44) and u_{rigid} values are

$$\begin{cases} u_{\text{Rigid,HR}} = \infty \\ u_{\text{Rigid,VS}} = 2k_{\text{cb}}D^2/i_{\text{c}} \\ u_{\text{Rigid,VR}} = \infty \\ u_{\text{Rigid,FR}} = 2i_{\text{fb}}/i_{\text{c}} \\ u_{\text{Rigid,CR}} = 2i_{\text{cb}}/i_{\text{c}} \end{cases} \tag{49}$$

For all the five joint parameters, denote

$$\mu = \sqrt{\frac{0.05 + K_{\text{rigid}}^2\bar{\lambda}_0^2}{0.95\bar{\lambda}_0^2}} \tag{50}$$

Then, Eq. (46) becomes

$$K \le \mu \tag{51}$$

By substituting Eq. (47) into Eq. (51), it is obtained

$$u \ge \frac{4.1(1-\mu)}{(1.636\mu - 1.145)} \tag{52}$$

Let

$$u_{\mathrm{B}} = \frac{4.1(1-\mu)}{(1.636\mu - 1.145)} \tag{53}$$

383 By substituting u_{B} into Eq. (44), the boundary limit values for the five joint parameters are
384 obtained as

$$\begin{cases} B_{\mathrm{HR}} = (u_{\mathrm{B}} - 6 - 2k_{\mathrm{fb}}D^2/i_{\mathrm{c}})/2 \\ B_{\mathrm{VS}} = 2/(2k_{\mathrm{cb}}D^2/i_{\mathrm{c}}u_{\mathrm{B}} - 1) \\ B_{\mathrm{VR}} = u_{\mathrm{B}} \\ B_{\mathrm{FR}} = 2/(2i_{\mathrm{fb}}/i_{\mathrm{c}}u_{\mathrm{B}} - 1) \\ B_{\mathrm{CR}} = 2/(2i_{\mathrm{cb}}/i_{\mathrm{c}}u_{\mathrm{B}} - 1) \end{cases} \tag{54}$$

385 According to Eq.(54), it is observed that all of the boundary limit values are dependent on
386 the column section. In addition, B_{HR} is dependent on the properties of the floor beam, B_{VS} is
387 dependent on the properties of the ceiling beam, B_{FR} is dependent on the floor beam properties,
388 and B_{CR} is dependent on the ceiling beam properties.

389 Figure 9 shows the steps to obtain the boundary limit values for the five joint parameters,
390 applying the given sizes of the module and member sections. The boundary limit values
391 calculated using Eq.(54) are listed in Table 4. These values are almost the same as those listed
392 in Table 2, indicating the effectiveness of the evaluation formulas proposed for the limit value
393 of the boundary.

394 For all the five joint parameters, the rigid and non-rigid boundary limit values decreases as
395 the column size increases or the slenderness decreases. A series of conservative boundary limit
396 values can be set as 1.6, 2.3, 14, 2.3, and 2.3 for the five joint parameters HR, VS, VR, FR, and
397 CR, respectively.

398

Step 1: Given L, H, column section, beam sections, obtain i_c, i_{fb}, i_{cb}, k_{cb}, $\bar{\lambda}_0^2$, D

Step 2: Obtain the column end restraint factors when joint parameters are rigid by Eq. (49)

$$\begin{cases} u_{\text{Rigid,HR}} = \infty \\ u_{\text{Rigid,VS}} = 2k_{cb}\,D^2/i_c \\ u_{\text{Rigid,VR}} = \infty \\ u_{\text{Rigid,FR}} = 2\,i_{fb}/i_c \\ u_{\text{Rigid,CR}} = 2\,i_{cb}/i_c \end{cases}$$

Step 3: Obtain the effective length ratio by Eq. (48)

$$K_{\text{rigid}} = \frac{1+0.145\frac{8}{4+u_{\text{rigid}}}-0.265\frac{4}{4+u_{\text{rigid}}}}{2-0.364\frac{8}{4+u_{\text{rigid}}}-0.247\frac{4}{4+u_{\text{rigid}}}}$$

Step 4: Obtain the parameters by Eq. (50) and (53)

$$\mu = \sqrt{\frac{0.05+K_{\text{rigid}}^2\bar{\lambda}_0^2}{0.95\bar{\lambda}_0^2}} \text{ and } u_B = \frac{4.1(1-\mu)}{(1.636\mu-1.145)}$$

Step 5: Obtain the boundary limit values by Eq. (54)

$$\begin{cases} B_{HR} = (u_B - 6 - k_{fb}\,D^2/i_c)/2 \\ B_{VS} = 2/(2k_{cb}\,D^2/i_c u_B - 1) \\ B_{VR} = u_B \\ B_{FR} = 2/(2\,i_{fb}/i_c u_B - 1) \\ B_{CR} = 2/(2\,i_{cb}/i_c u_B - 1) \end{cases}$$

Figure 9. Steps to obtain the boundary limit values for the five joint parameters depending on the sizes of the module and member sections.

Table 4. Rigid and non-rigid boundary values for B_{HR}, B_{VS}, B_{VR}, B_{FR}, and B_{CR} by boundary limit formulas

	SHS 90×5 ($\bar{\lambda}_0 = 1.15$)	SHS 100×6.3 ($\bar{\lambda}_0 = 1.04$)	SHS 120×6.3 ($\bar{\lambda}_0 = 0.86$)	SHS 160×8 ($\bar{\lambda}_0 = 0.64$)	SHS 220×10 ($\bar{\lambda}_0 = 0.46$)
B_{HR}	1.6	1.6	0.6	0	0
B_{VS}	2.3	2.1	1.1	0	0
B_{VR}	14	12	9	5	2
B_{FR}	2.3	2.1	1.4	0.4	0
B_{CR}	2.3	2.1	1.1	0	0

5 Verification

Two examples are presented to validate the effectiveness of the proposed boundaries. The first one is a low-rise steel MiC structure and the second one is a high-rise steel MiC structure braced by a concrete core.

5.1 Descriptions of the steel MiC buildings

The five-story steel MiC structure is similar to that shown in Figure 4(a). Each story consists of five modules, of which the left and right modules are braced with angled steel profiles to provide adequate lateral stiffness and resistance. The joint region is shown in Figure 4(c). Considering only the gravity loads, the two middlemost bays in Figure 10 were used to study the effect of the joint properties. The cross-sectional properties of the frame are SHS 90×5 for columns, RHS 140×80×8 for floor beams, and SHS 80×5 for ceiling beams, as shown in Table 5.

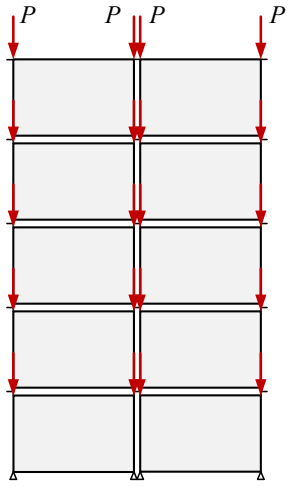

Figure 10. The two middle-most bays in the five-story structure.

Table 5. Cross-sectional properties for the five-story steel MiC frame

Member	Section type	Second moment of area (10^6 mm^4)	Bending stiffness EI/L^* or EI/H (kNm)	Axial stiffness EA/L^* (kN/m)

Floor beam	RHS 140×80×8	7.763	320	131634
Ceiling beam	SHS 80×5	1.314	54	59163.2
Column	SHS 90×5	3.356	137	/

*L = 5 m, H = 3 m.

According to the approach presented in Figure 9, the calculated boundary limit values are 1.6, 2.3, 14.0, 2.3, and 0.9. The carrying capacity of the structure with all rigid joint parameters, as well as that with the boundary limit values, was evaluated using the finite element model described in Section 5.2.

The high-rise steel MiC structure is a 40-story residential modular building, as reported by Chua et al. (2020) [11], where the modules are arranged around a central concrete core that provides lateral resistance, as shown in Figure 11(a). The data for the modular beams and columns at the bottom story are listed in Table 6.

Assuming that the concrete core is able to provide adequate lateral stiffness, the building model was simplified as a plane frame with two modules in the horizontal direction and 40 modules in the vertical direction, as shown in Figure 11(b). The lateral movement on the right side of the model was restrained to reflect the strong support of the concrete core.

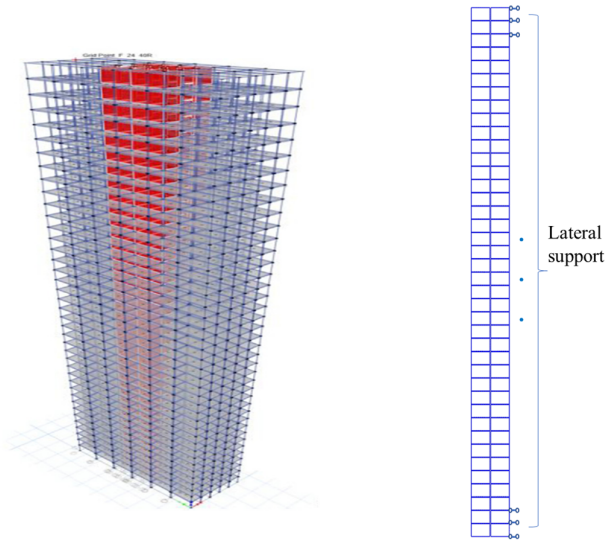

(a) (b)

Figure 11. The 40-storey modular building: (a) 3D view (Chua et al. 2020); (b) model adopted in the analysis.

Table 6. Design data for the 40-story steel MiC structure

Member	Section type	Second moment of area (10^6 mm^4)	Bending stiffness EI/L^* or EI/H (kNm)	Axial stiffness EA/L^* (kN/m)
Floor beam	RHS 160×80×8.3	9.032	310	92923
Ceiling beam	SHS 80×5	1.314	45	49303
Column	RHS 300×200×16	173.9	12173	/

*L = 6 m, H = 3.3 m.

According to the approach presented in Figure 9, the calculated boundary limit values are 0, 0, 0.9, 0, and 0, for B_{HR}, B_{VS}, B_{VR}, B_{FR}, and B_{CR}, respectively. The carrying capacity of the

441 structure with all rigid joint parameters, as well as that with the boundary limit values, will be
442 evaluated using the finite element model described in Section 5.2.

443 ## 5.2 Finite element model

444 ### *5.2.1 Material and elements*

445 The OpenSees platform [44] was used to study the behavior of the steel MiC structure using
446 geometrical and material nonlinearities with the imperfection analyses. The columns at the first
447 and second stories were evenly meshed as 10 and 5 *dispbeamcolumn* elements, respectively, to
448 model the spread of plasticity throughout the cross-sections and along the members. The floor
449 and ceiling beams were meshed using five *dispbeamcolumn* elements. A co-rotational
450 formulation was adopted for the modular columns to model the second-order effect for the
451 modular columns under large deformations. A fiber section considering material nonlinearity
452 was assigned for each modular member. The residual stress pattern adopted by the ECCS [45]
453 to develop the buckling ratio in EN 1993-1-1 [46] was adopted here. While discretizing the
454 section, the exact round corner of the hollow section was modelled such that the strength obtained
455 by the model was close to the nominal value provided by the design tables. The steel material
456 was modelled as elastoplastic with isotropic strain hardening, and the hardening ratio was set to
457 0.01. The elastic modulus was set to 206 GPa, and the nominal yield stress was 355 MPa. The
458 initial out-of-straightness of the steel column was modeled assuming that the initial geometrical
459 imperfection varies sinusoidally with a maximum value of δ_H = 1/1000 at mid-height. For the
460 possible direction of the out-of-straightness, two situations were considered, namely, outward
461 left and right. Subsequently, the carrying capacity was taken as the smaller value from the two
462 models. Out-of-plumbness was not considered, as Clarke et al. [47] found this to have a
463 negligible effect on the frame behavior.

464 *5.2.2 Joints*

465 Both inter- and intra-module joints were modelled using *twoNodeLink* element in OpenSees,
466 which has three degrees of freedom, namely, axial, shear, and rotational. A very stiff elastic
467 property was assigned for the axial and shear directions using a uniaxial elastic material, where
468 the stiffness of the rotational degrees of freedom varies depending on the analysis scenarios.

469 *5.2.3 Loading conditions*

470 In this study, the lateral force was assumed to be entirely supported by the bracing system;
471 hence, the steel modules were stressed only by the gravitational loads. Vertical point loads in the
472 gravitational direction were added to the top of each modular column. All loads were added
473 simultaneously until the failure of the structure and the carrying capacity was defined as the
474 maximum axial load sustained by a bottom modular column. Note that only the inelastic flexural
475 buckling failure of the column was considered, assuming that the beams and joints have a
476 sufficient ductility.

477 ## 5.3 Results

478 The failure model of the five-story steel MiC structure is shown in Figure 12(a), which
479 presents a typical flexural buckling phenomenon in the bottom column. The carrying capacities
480 for the different joint properties are listed in Table 7. Adopting the rigid joint parameters, the
481 carrying capacity could be increased to 512.6 kN. When using the proposed boundary limits, the
482 carrying capacity was 494.4 kN, or 96.4% of the value assuming rigid properties for both inter-
483 and intra-module joints.

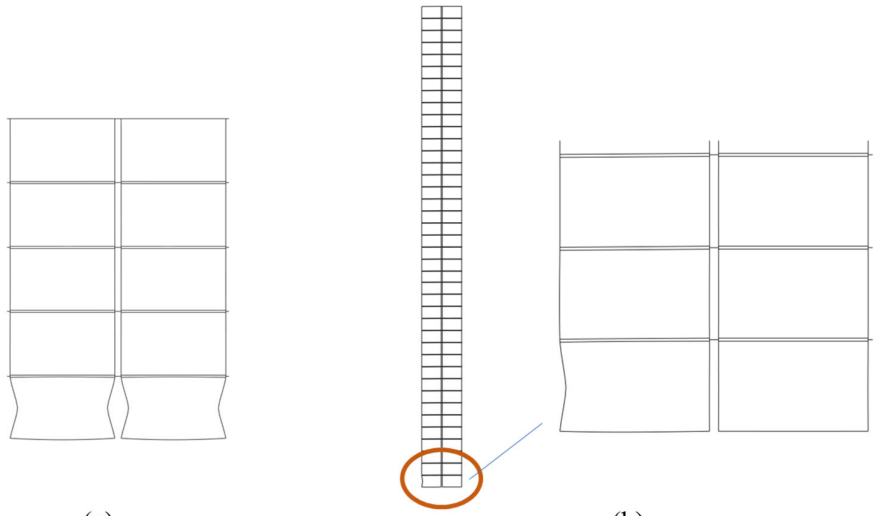

Figure 12. Typical failure modes: (a) the five-storey steel MiC structure; (b) the forty-storey steel MiC structure.

Table 7. Carrying capacity of the five-story MiC structure assuming different joint properties

	Inter-module joints			Intra-module joints		Carrying capacity (kN)	Relative capacity with respect to rigid-rigid assumption
	$\bar{S}_{HR}$	$\bar{S}_{VS}$	$\bar{S}_{VR}$	$\bar{S}_{FR}$	$\bar{S}_{CR}$		
Rigid	Rigid	Rigid	Rigid	Rigid	Rigid	512.6	100%
Boundary limit values	1.6	1.2	14	2.5	2.5	494.4	96.4%

The failure mode of the forty-storey steel MiC structure is shown in Figure 12(b), where the typical flexural buckling mode of the bottom column is presented. The carrying capacities with respect to different joint properties are listed in Table 8. The difference in the capacity values with various joint modelling assumptions was very small; within 1%. Therefore, the proposed boundary limit is deemed applicable.

Table 8. Carrying capacity of the forty-story structure

	Inter-module joints			Intra-module joints		Carrying capacity (kN)	Relative capacity with respect to rigid-rigid assumption
	$\bar{S}_{\mathrm{HR}}$	$\bar{S}_{\mathrm{VS}}$	$\bar{S}_{\mathrm{VR}}$	$\bar{S}_{\mathrm{FR}}$	$\bar{S}_{\mathrm{CR}}$		
Rigid	Rigid	Rigid	Rigid	Rigid	Rigid	4955	100%
Boundary limit values	0	0	0.9	0	0	4930	99.5%

6. Conclusions

This study aims to investigate the effect of stiffness properties of intra- and inter-module joints on the structural carrying capacity of braced steel MiC structures and propose a joint classification system to facilitate design.

First, the study demonstrated the semi-rigidity of the joint region of steel MiC structures. Then, five key joint parameters were identified for classification: the rotational behavior of horizontal inter-module joints (S_{HR}), shear behavior of vertical inter-module joints (S_{VS}), rotational behavior of vertical inter-module joints (S_{VR}), rotational behavior of intra-module floor beam-column joints (S_{FR}), and rotational behavior of intra-module ceiling beam-column joints (S_{CR}). A reference substructure with these five parameters was adopted for performance evaluation. The rotational restraint effect factors on the bottom modular column in the reference substructure were derived explicitly based on the five joint parameters, as well as the column and beam section properties. Subsequently, the carrying capacity of the structure was evaluated using the Merchant function. The effects of different joint parameter values on the carrying capacity were investigated using the sensitivity analysis, and the critical joint configurations for

each joint parameter were determined. Then, the classification boundary limit values for inter- and intra-module joints in non-sway steel MiC structures were derived according to the respective critical joint configurations. The proposed boundary classification system is dependent on the properties of the modular columns and can be calculated based on explicit formulas.

The joint classification system was validated using the examples of a low-rise steel-braced and high-rise braced steel MiC structures, where the carrying capacity was evaluated applying the geometrical and material nonlinearities with the imperfection analyses conducted using the OpenSees platform. Thereby the proposed classification system can be used when designing the steel MiC structures.

Nomenclature

A_{fb}, A_{cb}	= Cross-section areas of the floor beam and ceiling beam
B_{FR}, B_{CR}	= Boundary limit values for the rotational stiffness of floor and ceiling beam-column joints
B_{HR}, B_{VR}	= Boundary limit values for the rotational stiffness of vertical and horizontal inter-module joints
B_{VR}	= Boundary limit value for the shear behavior of vertical inter-module joints
D	= A half of the distance between the center axiss of adjacent floor beam and ceiling beam
E	= Elastic modulus of steel material
H	= Height of the module
I_{c}, I_{fb}, I_{cb}	= Moments of inertia of column, floor beam, and ceiling beam

i_c, i_{fb}, i_{cb} = Element bending stiffnesses of column, floor beam, and ceiling beam, $i_c = EI_c/H$, $i_{fb} = EI_{fb}/L$, $i_{cb} = EI_{cb}/L$

K = Effect length ratio

k_{fb}, k_{cb} = Element axial stiffnesses of the floor beam and ceiling beam, $k_{fb} = EA_{fb}/L$, $k_{cb} = EA_{cb}/L$

L = Length of the module

S_{FR}, S_{CR} = Rotational stiffness values of floor and ceiling beam-column joints

S_{VR}, S_{HR} = Rotational stiffness values of vertical and horizontal inter-module joints

S_{VS} = Shear stiffness value of vertical inter-module joints

$\bar{S}_{FR}$, $\bar{S}_{CR}$ = Relative rotational stiffness values of floor and ceiling beam-column joints, $\bar{S}_{FR} = S_{FR}/i_c$, $\bar{S}_{CR} = S_{CR}/i_c$

$\bar{S}_{VR}$, $\bar{S}_{HR}$ = Relative rotational stiffness values of vertical and horizontal inter-module joints, $\bar{S}_{VR} = S_{VR}/i_c$, $\bar{S}_{HR} = S_{HR}/i_c$

$\bar{S}_{VS}$ = Relative shear stiffness value of vertical inter-module joints,

CRediT authorship contribution statement

Xiao-Huang-Can He: Concept, Investigation, Writing – original draft, Funding acquisition. **Tak-Ming Chan**: Concept, Writing – review & editing, Supervision.

Declaration of Competing Interest

The authors declare that they have no known competing financial interests or personal relationships that could have influenced the results reported in this study.

Acknowledgement

The authors sincerely acknowledge the support provided by the Starting Research Fund of Guangxi University for high-level innovation talent.

Reference

[1] Z. Duan, B. He, Z. Yuan, J. Ruan, X. Zhang, Application of BIM Technology in Nanjing Honeycomb Hotel, IOP Conf. Ser., Earth Environ. Sci. (UK) 218 (2019) 012054.

[2] Construction industry council, InnoCell, 2020. https://mic.cic.hk/en/ProjectsInHongKong/1.

[3] H.K. Park, J.-H. Ock, Unit modular in-fill construction method for high-rise buildings, KSCE Journal of Civil Engineering 20(4) (2015) 1201-1210.

[4] H. Rajanayagam, K. Poologanathan, P. Gatheeshgar, G.E. Varelis, P. Sherlock, B. Nagaratnam, P. Hackney, A-State-Of-The-Art review on modular building connections, Structures 34 (2021) 1903-1922.

[5] A.W. Lacey, W. Chen, H. Hao, K. Bi, Review of bolted inter-module connections in modular steel buildings, Journal of Building Engineering 23 (2019) 207-219.

[6] M. Farajian, P. Sharafi, K. Kildashti, The influence of inter-module connections on the effective length of columns in multi-story modular steel frames, Journal of Constructional Steel Research 177 (2021).

[7] X. Zhai, X. Zha, D. Chen, Elastic stability of unbraced plate-type modular steel frames with semi-rigid corner connections, Journal of Constructional Steel Research 192 (2022).

[8] G.-Q. Li, K. Cao, Y. Lu, J. Jiang, Effective length factor of columns in non-sway modular steel buildings, Advanced Steel Construction 13(4) (2017) 412-426.

[9] G.-Q. Li, K. Cao, Y. Lu, Column effective lengths in sway-permitted modular steel-frame buildings, Proceedings of the Institution of Civil Engineers - Structures and Buildings 172(1) (2019) 30-41.

[10] A.W. Lacey, W. Chen, H. Hao, K. Bi, Effect of inter-module connection stiffness on structural response of a modular steel building subjected to wind and earthquake load, Engineering Structures 213 (2020).

[11] Y.S. Chua, J.Y.R. Liew, S.D. Pang, Modelling of connections and lateral behavior of high-rise modular steel buildings, Journal of Constructional Steel Research 166 (2020) 1-17.

[12] M. Alembagheri, P. Sharafi, M. Rashidi, Experimental and Numerical Study on the Robustness of Full-Scale Volumetric Steel Module under Sudden Support Removal Scenarios, Journal of Performance of Constructed Facilities 36(1) (2022).

[13] S. Srisangeerthanan, M.J. Hashemi, P. Rajeev, E. Gad, S. Fernando, Review of performance requirements for inter-module connections in multi-story modular buildings, Journal of Building Engineering 28 (2020) 101087.

[14] A.J. Styles, F.J. Luo, Y. Bai, J.B. Murray-Parkes, Effects of joint rotational stiffness on structural responses of multi-story modular buildings, 2016 International Conference on Smart Infrastructure and Construction, ICSIC 2016, ICE Publishing, 2016, pp. 457-462.

[15] X.H.C. He, T.M. Chan, K.F. Chung, Effect of inter-module connections on progressive collapse behaviour of MiC structures, Journal of Constructional Steel Research 185 (2021) 106823.

572 [16] Y.-F. Lyu, G.-Q. Li, K. Cao, S.-Y. Zhai, Y.-B. Wang, L. Mao, M.-m. Ran, Bending
573 behavior of splice connection for corner-supported steel modular buildings, Engineering
574 Structures 250 (2022).
575 [17] F.J. Luo, Y. Bai, J. Hou, Y. Huang, Progressive collapse analysis and structural
576 robustness of steel-framed modular buildings, Engineering Failure Analysis 104 (2019) 643-656.
577 [18] EN 1993-1-8, Eurocode 3: Design of steel structures - Part 1-8: Design of joints,
578 European Commitee for Standardization (CEN), Brussels, 2005, pp. 1-133.
579 [19] R. Bjorhovde, A. Colson, J. Brozzetti, Classfication system for beam-to-column
580 connections, Journal of Structural Engineering 116(11) (1990) 3059-3076.
581 [20] M. Farajian, P. Sharafi, H. Eslamnia, K. Kildashti, Y. Bai, Classification of inter-
582 modular connections for stiffness and strength in sway corner-supported steel modular frames,
583 Journal of Constructional Steel Research 197 (2022) 107458.
584 [21] W.-F. Chen, N. Kishi, Semirigid steel beam-to-column connections: Data base and
585 modeling, Journal of Structural Engineering 115 (1989) 1.
586 [22] Y. Goto, S. Miyashita, Classification System for Rigid and Semirigid Connections,
587 Journal of Structural Engineering 124(7) (1998) 750-757.
588 [23] N. Kishi, R. Hasan, Study of Eurocode 3 steel connection classfication, Engineering
589 Structures 19(9) (1997) 772-779.
590 [24] D.A. Nethercot, T.Q. Li, B. Ahmed, Unified classification system for beam-to-column
591 connections, Journal of Constructional Steel Research 45(1) (1998) 39-65.
592 [25] F.S.K. Bijlaard, C.M. Steenhuis, Prediction of the influence of connection behaviour on
593 the strength, deformations and stability of frames, by classification of connections, in: R.
594 Bjorhovde, G. Haaijer, A. Colson, J.W.B. Stark (Eds.) Connections in steel structures, American
595 institute of steel construction, Chigaco, 1992.
596 [26] R. Hasana, N. Kishib, W.-F. Chen, A new nonlinear connection classification system,
597 Journal of Constructional Steel Research 47 (1998) 119-140.
598 [27] I. Birkelanda, A. Aalberga, S. Kvam, Classification boundaries for stiffness of beam-to-
599 column Joints and column bases, Nordic Steel Construction Conference 2012, Hotel Bristol,
600 Oslo, Norway, 2012, pp. 1-12.
601 [28] D.-A. Corfar, K.D. Tsavdaridis, A comprehensive review and classification of inter-
602 module connections for hot-rolled steel modular building systems, Journal of Building
603 Engineering 50 (2022).
604 [29] X.-M. Dai, L. Zong, Y. Ding, Z.-X. Li, Experimental study on seismic behavior of a
605 novel plug-in self-lock joint for modular steel construction, Engineering Structures 181 (2019)
606 143-164.
607 [30] Y. Liu, Z. Chen, J. Liu, Y. Bai, X. Zhong, X. Wang, Lateral stiffness evaluation on
608 corner-supported thin walled modular steel structures, Thin-Walled Structures 157 (2020)
609 106967.
610 [31] A.W. Lacey, W. Chen, H. Hao, K. Bi, F.J. Tallowin, Shear behaviour of post-tensioned
611 inter-module connection for modular steel buildings, Journal of Constructional Steel Research
612 162 (2019) 105707.
613 [32] R. Sanches, O. Mercan, B. Roberts, Experimental investigations of vertical post-
614 tensioned connection for modular steel structures, Engineering Structures 175 (2018) 776-789.
615 [33] H. Yang, Performance analysis of semi-rigid connections in prefabricated high-rise steel
616 structures, Structures 28 (2020) 837-846.

[34] S.V. Sendanayake, D.P. Thambiratnam, N. Perera, T. Chan, S. Aghdamy, Seismic mitigation of steel modular building structures through innovative inter-modular connections, Heliyon 5(11) (2019) e02751.
[35] M. Lawson, R. Ogden, C. Goodier, Design in modular construction, CRC Press, Boca Raton, 2014.
[36] A.W. Lacey, W. Chen, H. Hao, K. Bi, New interlocking inter-module connection for modular steel buildings: Experimental and numerical studies, Engineering Structures 198 (2019) 109465.
[37] P. Chain, Prefabricated prefinished volumetric construction (PPVC) in Singopore: NTU case studies, International Conference on Modular Integrated Construction, Kowloon, Hong Kong, 2018.
[38] E.-F. Deng, J.-Y. Lian, Z. Zhang, H. Qian, G.-C. Zhang, P. Zhang, S.A. Sheikh, Axial mechanical behavior of an innovative liftable connection for modular steel construction, Thin-Walled Structures 182 (2023).
[39] E. Bazarchi, A. Davaran, C.P. Lamarche, N. Roy, S. Parent, Experimental and numerical investigation of a novel vertically unconstrained steel inter-modular connection, Thin-Walled Structures 183 (2023).
[40] J. Dhanapal, H. Ghaednia, S. Das, J. Velocci, Behavior of thin-walled beam-column modular connection subject to bending load, Thin-Walled Structures 149 (2020) 106536.
[41] F. Zhao, Y. Yu, S. Lin, F. Ding, Evaluation of the working mechanisms and simplified models of endplate-type inter-module connections, Structures 32 (2021) 562-577.
[42] W. Merchant, The failure load of rigid jointed frameworks as influenced by stability, The Structural Engineer 32(7) (1954) 185-190.
[43] J.-P. Jaspart, F. Wald, K. Weynand, N. Gresnigt, Steel column base classification, HERON 53 (2008).
[44] S. Mazzoni, F. McKenna, M.H. Scott, G.L. Fenves, The open system for earthquake engineering simulation (OpenSEES) user command-language manual, Citeseer2006.
[45] ECCS, Manual on stability of steel strucutres, 1976.
[46] EN 1993-1-1, Eurocode 3: Design of steel structures - Part 1-1: General rules and rules for buildings, European Commitee for Standardization (CEN), Brussels, 2005.
[47] M.J. Clarke, R.Q. Bridge, G.J. Hancock, N.S. Trahair, Advanced Analysis of Steel Building Frames, Journal of Constructional Steel Research 23(1-3) (1992) 1-29.